Giant, 29, 2026, 100413

Electromechanical transduction and actuation performance of P(VDF-TrFE)/P(VDF-TrFE-CTFE) electroactive polymer blends

Full-length article

Giulio Gallucci*, Andres Hunt

Department of Precision and Microsystems Engineering, Faculty of Mechanical Engineering, Delft University of Technology, Mekelweg 2, Delft 2628 CD, the Netherlands

Keywords: Electroactive polymers, Polymer blends, P(VDF-TrFE-CTFE), P(VDF-TrFE), Electromechanical transduction, Unimorph actuators

Electroactive polymer (EAP) blends of relaxor-ferroelectric P(VDF-TrFE-CTFE) and ferroelectric P(VDF-TrFE) were investigated for enhanced electromechanical transduction. Blends containing 0–30 wt% copolymer were stencil-printed onto thin steel substrates for characterization in dielectric, mechanical, and structural properties, while unimorph cantilever actuators were produced for characterizing transduction. Copolymer addition increased the Young's modulus and promoted ferroelectric ordering while reducing dielectric permittivity and dielectric loss in the EAPs. Maximum quasi-static actuation displacements improved from 8.1 mm at 50 V/μm in neat terpolymer samples to 9.2 mm at 48.3 V/μm in 10 wt% blends, that showed the highest overall improvements. At 20 V/μm, the maximum deflection and transducer efficiency respectively reached 2.1 mm and 0.0576%, corresponding to 94.4% and 357% improvements over the pure terpolymer. Under dynamic operation, the 10 wt% blends also produced the highest resonant displacement (2.30 mm at 6.7 V/μm), yielding a 53.7% improvement over the pure terpolymer. Higher copolymer contents (20 and 30 wt%) further increased in stiffness and unimorph efficiency but showed lower displacement due to reduced EAP film stress. These results demonstrate that polymer blending is an effective strategy to tune transduction performance in PVDF-based unimorph actuators, with further gains expected through optimization of blend composition and actuator design.

1 Introduction

Electroactive polymer (EAP)-based transducers have attracted growing interest as alternatives to conventional actuation technologies because they are lightweight, mechanically flexible, simple in construction, and able to generate comparatively large electrically induced strains [1,2]. Among EAPs, poly(vinylidene fluoride) (PVDF) and its derivatives have been extensively studied in haptics, soft robotics, and microfluidic devices due to their strong electromechanical response, combined with good chemical stability and processability [3–8].

Incorporation of TrFE (trifluoroethylene) monomer into the PVDF chain yields ferroelectric P(VDF-TrFE) copolymers

* Corresponding author.
E-mail address: G.Gallucci@tudelft.nl (G. Gallucci).
Received 6 May 2026; Received in revised form 16 July 2026; Accepted 28 July 2026

 https://doi.org/10.1016/j.giant.2026.100413

[9,10], while further addition of bulky termonomers such as CFE (chlorofluoroethylene) or CTFE (chlorotrifluoroethylene) introduces structural defects that induce relaxor-ferroelectric behavior [11,12]. The resulting terpolymers, P(VDF-TrFE-CFE) and P(VDF-TrFE-CTFE), exhibit slim hysteresis loops and large electrostrictive response, described by the quadratic strain-field relation $S = ME^2$, where M is the apparent electrostrictive coefficient [13].

Relaxor terpolymers have been shown to exhibit lower Young's modulus and crystallinity than P(VDF-TrFE), but higher dielectric permittivity and larger field-induced strains, which have motivated extensive research into their use in actuators and transducers [14]. One limitation, however, is the high electric field (e.g., >90 V/μm) often required to achieve significant strain [15]. Depending on actuator design, this can lead to limited output displacement and hinder practical application.

Several strategies have been explored to improve actuation in these terpolymers. Small amounts of plasticizers or conductive nanofillers have been reported to increase low-field strain through modifications of dielectric, mechanical, and structural properties [16–18]. However, such improvements often come at the expense of reduced breakdown strength and increased fabrication complexity. In conductive filler nanocomposites, the interfacial polarization and percolation effects that increase permittivity can also increase dielectric losses and intensify local electric fields when fillers are poorly dispersed, making surface functionalization and dispersion control critical [16,17]. Plasticizers offer a simpler route, but their concentration is limited by compatibility with the EAP matrix and by reduced breakdown strength due to increased charge transport and dielectric heterogeneity [7,19–21].

Another versatile approach is blending the terpolymers with other EAPs. Gorny *et al.* reported unchanged strain but improved energy density upon blending P(VDF-TrFE-CFE) with 2.5 wt% P(VDF-CTFE), reaching up to 0.73 J/cm^3 at 150 V/μm [22], while Chu *et al.* reported improved breakdown strength in similar blends containing 5 wt% P(VDF-CTFE) [23]. In both cases, the effect was attributed to the increase in Young's modulus of the blends.

P(VDF-TrFE) blending has been shown to improve quasi-static actuation in terpolymer-based unimorph bending actuators at room temperature and 60 °C, depending on the compositions of both the terpolymer and the copolymer [24,25].

Unimorph tip displacements have been reported to increase from 0.4 mm to 0.47 mm (110 V/μm, $L = 45$ mm) in terpolymer (3.8 mol% CFE) blends with 20 wt% P(VDF-TrFE) (55 mol% VDF), while increasing the VDF content of the copolymer to 75 mol% improved high-temperature actuation response (60 °C) [24].

Similar trends were recently observed in P(VDF-TrFE-CTFE)-based blends containing up to 20 wt% P(VDF-TrFE), increasing cantilever tip displacements from 0.41 mm to 0.49 mm for 10 wt% P(VDF-TrFE) actuators ($L = 45$ mm, 110 V/μm, 25 °C) [25]. Cantilever deflections were mapped to terpolymer and copolymer composition- and temperature-dependency, and one terpolymer composition (4.2 mol% CTFE) blended with two copolymers (75 and 55 mol% VDF) was studied in detail in terms of film stresses, strains, microstructure, and chain conformation.

While these are very promising results, more research is needed in terms of blend materials (constituent polymers and blend composition), their properties (mechanical, dielectric, structural, transduction) and implementation for actuation. This work investigates the dielectric, mechanical, structural and transduction properties of P(VDF-TrFE-CTFE) blends with P(VDF-TrFE) for actuation. P(VDF-TrFE) copolymer (70 mol% VDF) was blended with the terpolymer (8.6 mol% CTFE) in 0 to 30 wt% P(VDF-TrFE) compositions.

The blends were stencil-printed and integrated into unimorph bending cantilever actuators, as described in Sections 2.1 and 2.2. The effect of copolymer content (0–30 wt%) on dielectric properties, mechanical properties, local chain conformations and actuation performance was investigated through impedance analysis, nanoindentation, Fourier transform infrared spectroscopy (FTIR), and actuator characterization, including tip deflection, transverse strain, film stress, energy density, and transducer efficiency, as detailed in Section 2.3. The resulting material properties and actuator performance are then compared across blend compositions in Section 3, and the main conclusions are summarized in Section 4.

2 Materials and methods

2.1 Materials

P(VDF-TrFE-CTFE) terpolymer powder (Piezotech RT-TS, 8.6 mol% CTFE) and P(VDF-TrFE) copolymer powder (Piezotech FC30, 30 mol% TrFE) were obtained from Arkema, Germany. Methyl ethyl ketone (MEK), purchased from Sigma-Aldrich, was used as the solvent. A 10 μm thick steel foil (Hasberg, Germany) was used as both the flexible substrate and bottom electrode for the unimorph cantilever actuators, while a 350–400 nm thick gold leaf was used for the top electrode.

Separate terpolymer and copolymer solutions were first prepared in MEK by dissolving 8 g of polymer in 72 g of solvent. The solutions were then mixed and stirred (Stuart UC152 magnetic stirrer) for 2 h at room temperature to obtain P(VDF-TrFE)/P(VDF-TrFE-CTFE) blends containing 0, 10, 20, and 30 wt% P(VDF-TrFE).

2.2 Fabrication

Separate EAP samples were fabricated for experimental characterization of mechanical, dielectric and transduction properties. In the first step, EAP films of 45 μm and 100 μm thickness were stencil-printed onto 50 μm thick steel substrates, respectively for nanoindentation (Section 2.3.2) and dielectric (Section 2.3.3) characterization. These samples were also used for ATR-FTIR characterization (Section 2.3.4). For transduction and actuation characterization, 30 μm thick EAP films were stencil-printed on thin steel substrates (thickness 10 μm). The as-deposited EAP films were immediately covered with a glass Petri dish and left to dry at room temperature for 6 h, followed by thermal annealing at 110 °C for 3 h to improve crystallinity.

While nanoindentation samples did not require any further fabrication steps, the dielectric characterization samples were completed by applying a circular electrode (10 mm in diameter, 350–400 nm thickness) on top of the EAP layer via gold leaf transfer. A steel mask was fixed by permanent magnets to the EAP-on-steel samples, and then, gold leaf was placed over the mask and covered by a thin PTFE film to facilitate release. The stack

Fig. 1

T-shaped EAP unimorph cantilever actuators.

was pressed by hand, using a steel and foam block to uniformly distribute the pressure. The unimorph cantilever actuator samples fabrication followed the same procedure. The top electrode was defined by a rectangular stencil that left a ca 0.5 mm electrode-free perimeter at the edges of the 20 mm × 6.5 mm EAP film area to prevent electrical short-circuit with the steel substrate. The actuator outline (Fig. 1) was then released by femtosecond laser micromachining (Lasea LS Lab).

2.3 Characterization

2.3.1 Morphology

Morphology of the EAP films and unimorph actuators was investigated using scanning electron microscopy (JSM-6010LA, JEOL Ltd., Tokyo, Japan). Top-view and cross-sectional images were acquired at an accelerating voltage of 10 kV. Cross-sections of the samples were exposed using a femtosecond laser cutting (Lasea LS Lab, Pharos PH1 10W 1030 nm source).

2.3.2 Nanoindentation

Young's moduli of the EAP samples were evaluated via nanoindentation (Piuma, Optics11 Life) using a cantilever probe with a spherical tip (10.5 µm radius) and a stiffness of 203.4 N/m. Measurements were conducted in displacement-control mode, consisting of a loading phase at 1.1 µm/s, a 1 s hold phase, and an unloading phase at the same rate. At least 20 indentations were conducted over the surface of each sample (20 mm × 6.5 mm) for reliable measurement.

The Young's modulus Y was evaluated by fitting the Hertzian contact model to the loading segment of the indentation curves [26]:

$$P = \frac{4}{3}\frac{Y}{1-\nu^2}\sqrt{R}h^{3/2}, \tag{1}$$

where P is the applied load, R is the indenter tip radius, h is the indentation depth, and ν is the Poisson' ratio. A Poisson's ratio of $\nu = 0.48$ (reported for P(VDF-TrFE-CTFE) [27,28]) was used for all formulations and assumed not to vary significantly upon blending.

2.3.3 Impedance analysis

The dielectric properties of the terpolymer blends were characterized using a Keysight E5061B vector network analyzer (VNA) operated in impedance analysis mode [29,30]. The VNA was equipped with Kelvin clip test leads (RS-PRO 123–5979) and custom-made clamp with circular Ag contact electrodes (10 mm diameter). The disc-shaped area defined by the sample electrodes (Section 2.2) formed the parallel plate capacitor geometry for impedance measurements. The relative permittivity

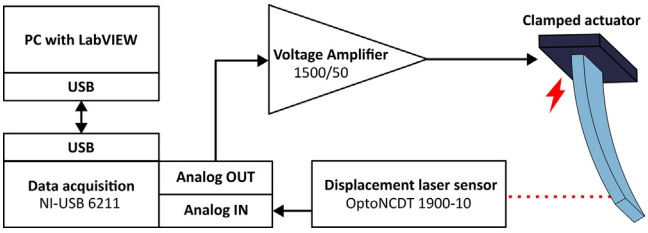

Fig. 2

Schematic of experimental setup for actuator characterization.

ε_r and dielectric loss tangent $\tan\delta$ were evaluated in the 100 Hz – 1 MHz frequency range (0.6 V excitation), respectively from

$$\varepsilon_r = \frac{Ct}{\varepsilon_0 A}, \tag{2}$$

where C is the capacitance (parallel configuration), t is the sample thickness, A is the electrode area, $\varepsilon_0 = 8.85 \times 10^{-12}\,\mathrm{F\,m^{-1}}$ is the permittivity of free space, and

$$\tan\delta = \frac{G}{2\pi f C}, \tag{3}$$

where G is the conductance and f is the frequency.

2.3.4 FTIR spectroscopy

ATR-FTIR spectroscopy was used to detect structural changes in the local chain conformations of the terpolymer films upon blending with P(VDF-TrFE). Spectra were collected using a Thermo Scientific Nicolet iS50 FTIR spectrometer in ATR mode over the 400–1500 $\mathrm{cm^{-1}}$ wavelength range, with a spectral resolution of 2 $\mathrm{cm^{-1}}$.

Measurements were performed at multiple spots on the 45 μm and 100 μm thick EAP films stencil-printed on steel (see Section 2.2) to verify consistency across film thicknesses. The absorbance spectra were baseline-corrected and normalized before comparison.

2.3.5 Actuation

Actuation and transduction properties of the EAP actuators and materials were characterized in quasi-static and dynamic actuation experiments using a custom-built set-up (see Fig. 2). The actuators were mechanically fixed using 3D-printed clamps (Elegoo standard resin 1.0, Elegoo Mars 3), equipped with copper tape electrodes for electrical connections. The actuators were driven by a high-voltage amplifier (HVA 1500/50, Smart Material Inc.) and their deflections were measured using a laser displacement sensor (Micro-Epsilon OptoNCDT 1900-10, 10 mm range, ±2 μm linearity, 0.4 µm repeatability) through a USB-6211 data acquisition unit (National Instruments). The experiments were controlled and data was stored using a custom LabVIEW 2018 (National Instruments) interface on a PC laptop (Lenovo X201i). Videos of all measurements were simultaneously recorded (SM-A266B/DS) with a millimeter paper background to estimate actuator deflection when they exceed the laser displacement sensor range (10 mm). Data was processed and plotted in MATLAB R2024b environment.

A sequence of three actuation experiments were performed on each sample using unipolar sinusoidal excitation: (i) quasi-static

actuation at 0.1 Hz, 200 V; (ii) frequency response measurements at 200 V in the 1 Hz – 40 Hz interval (at 49 individual logarithmically spaced frequencies), extended up to 60 Hz for stiffer samples; and (iii) actuation at incrementally increasing voltage (at 1 Hz, 10 s, 25 V increments) up to the amplifier voltage limit (1.5 kV) or sample breakdown.

The field-induced in-plane strain S (i.e., the transverse strain) was estimated from the quasi-static tip deflections δ using the small deflection model for a two-layer unimorph cantilever, in which bending arises from the passive substrate constraining the expansion of the active layer [31,32]:

$$\delta = \frac{3L^2}{2t} \cdot \frac{2AB(1+B)^2}{A^2B^4 + 2A(2B + 3B^2 + 2B^3) + 1} \cdot S, \tag{4}$$

where L and t respectively are the unimorph length and total thickness, $A = Y_{sub}/Y_{EAP}$ is the ratio of the substrate and EAP layers Young's moduli, and $B = t_{sub}/t_{EAP}$ is the ratio of their thicknesses. Based on the actuator design and substrate properties, $L = 20\ mm$, $Y_{sub} = 200\ GPa$ and $t_{sub} = 10\ \mu m$. The resulting transverse strains were further used to determine the EAP film stresses $\sigma = Y_{EAP}S$ and elastic energy densities $U_S = \frac{1}{2}Y_{EAP}S^2$, while the actuator transduction efficiencies k_u^2 were estimated using the analytical formulation derived by Wang *et al.* for unimorph benders [33]:

$$k_u^2 = \frac{9k_{EAP}^2}{4} \cdot \frac{A^2B^2(1+B)^2}{(AB+1)\left[A^2B^4 + 2A(2B + 3B^2 + 2B^3) + 1 - k_{EAP}^2 AB(AB^3+1)\right]} \tag{5}$$

where $k_{EAP}^2 = Y_{EAP}S^2/(Y_{EAP}S^2 + \varepsilon_r\varepsilon_0E^2)$ denotes the electromechanical coupling factor of the EAP [7]. Since Eqs. (4) and (5) are based on a small-deflection approximation, the material strains, film stresses and actuator efficiencies are only extracted for $\delta \leq 3$ mm in this study (coherent with prior research [7,34]).

3 Results and discussion

3.1 Fabrication

Stencil-printing the EAP films on steel substrates yielded a similar behavior for all inks, producing continuous EAP films with a visually translucent surface. Actuator fabrication produced EAP films with a thickness of 30 µm, allowing to deliver high field strengths of up to 50 V/µm. Thicker films were used for dielectric and ATR-FTIR characterization since the delicate films respectively needed to make contact with the Kelvin clip electrodes (Section 2.3.3) and the ATR crystal (Section 2.3.4). In nanoindentation (Section 2.3.2), thicker films were necessary to prevent measurement error due to the stiff steel substrate.

As described in Section 2.2, it was important to immediately cover the deposited films with a glass Petri dish and allow MEK to slowly evaporate at room temperature, resulting in dense surface morphologies shown in Fig. 3a. In contrast, uncovered samples exhibited surface drying, observable as rapid whitening of the film surface within the first minutes after printing, and consistently developed porous cellular morphology (Fig. 3b). This has previously been associated with rapid solvent evaporation (MEK boils at 80 °C), humidity-induced pore formation and phase separation during drying [35–38]. The denser surface morphology observed in the covered samples can therefore be attributed to the reduced MEK evaporation rate in the solvent-rich atmosphere and the reduced humidity-driven pore formation. Higher boiling point polar solvents such as N,N-dimethylformamide (DMF) or dimethyl sulfoxide (DMSO) could therefore be explored in future studies to gain further control over drying kinetics and film density.

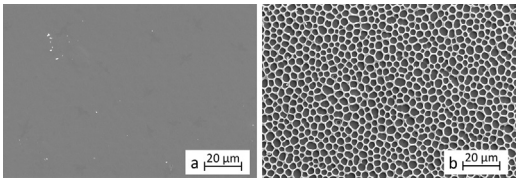

Fig. 3

Comparison of surface morphology in neat P(VDF-TrFE-CTFE) films that were covered (a) and uncovered (b) during solvent evaporation.

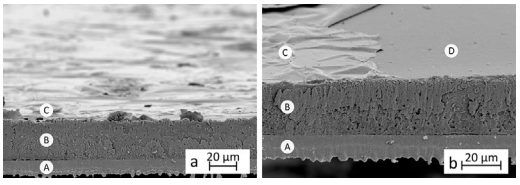

Fig. 4

Layered structure of the unimorph actuator cross-sections (a) in the middle of the sample, and (b) at the top electrode boundary (near the edge EAP layer boundary). Annotations: A - steel substrate, B - EAP layer, C - gold leaf top electrode, and D - electrode-free EAP surface.

Unimorph actuator samples are shown in Fig. 1. After release, all samples exhibited a small zero-field curvature, attributed to residual stresses generated during fabrication. Such curvature has been reported in unimorph actuators as a consequence of residual stresses in the actuator layered structure after thermal treatment [32,39]. Deflections were measured with respect to the zero-field shape and the applied voltage caused actuation towards straight configuration (see Section 3.5). Remaining in the vicinity of a straight shape allowed to ignore non-linearities between tip deflection and material strain.

SEM images of the unimorph actuator cross-sections are shown in Fig. 4 (see Section 2.3), indicating a well-defined interface between the 30 µm EAP layer and the 10 µm steel bottom electrode, as well as good adhesion of the gold leaf top electrode to the smooth EAP surface. In the middle of the sample (Fig. 4a) the EAP layer is uniform in thickness, while an increase is observed in EAP thickness near the edge of the sample (Fig. 4b). This is likely caused by meniscus formation at the stencil boundaries during MEK evaporation (see Section 2.2).

3.2 Mechanical properties

Nanoindentation measurements were performed according to Section 2.3.2 and are summarized in Fig. 5. This approach enabled direct measurement of the Young's modulus of the EAP films on steel, closely reflecting the respective films within the actuators. Macroscopic tensile testing would require free-standing samples

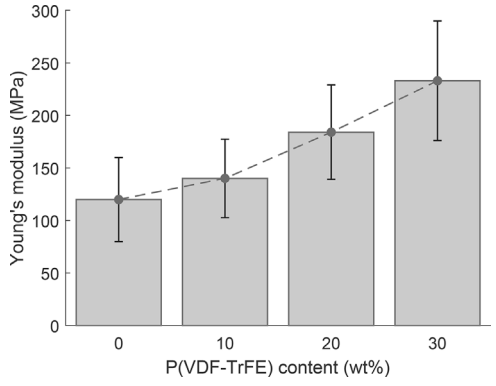

Fig. 5

Young's moduli of the P(VDF-TrFE)/P(VDF-TrFE-CTFE) blends from nanoindentation experiments at different blend ratios.

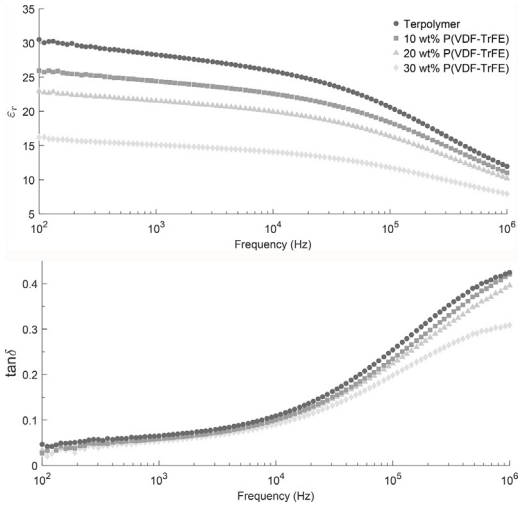

Fig. 6

Dielectric permittivity (ε_r) and loss tangent (tanδ) measurement results for all four EAP formulations.

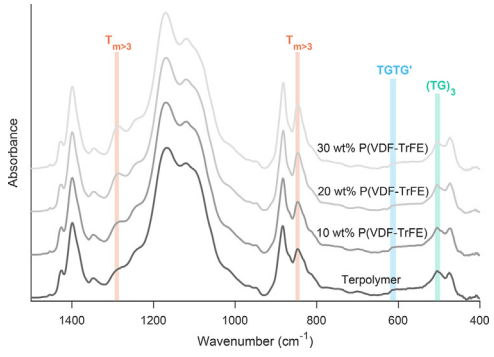

Fig. 7

ATR-FTIR absorbance spectra of the neat terpolymer and its blends with P(VDF-TrFE).

with sufficient thickness and gauge area that may exhibit slightly different effective Young's moduli and are impractical to fabricate.

The EAP Young's modulus gradually increased upon blending with P(VDF-TrFE), from 120 MPa for the neat terpolymer to 140, 184, and 233 MPa for the 10, 20, and 30 wt% blends, respectively. The increase was modest at 10 wt% and became more pronounced at higher copolymer loadings, indicating progressive stiffening upon blending. P(VDF-TrFE) copolymers have been shown to generally exhibit higher crystallinity and stiffness than relaxor terpolymers [14], explaining why incorporation of the copolymer into the relaxor matrix increases the overall Young's modulus. Similar stiffening upon P(VDF-TrFE) addition has been reported in blend studies of both P(VDF-TrFE-CFE) and P(VDF-TrFE-CTFE), with the magnitude of the effect depending on the terpolymer species and copolymer content [24,25].

3.3 Dielectric properties

Relative permittivity ε_r and dielectric loss tangent $\tan\delta$ of the EAP blends were evaluated at room temperature over the 100 Hz–1 MHz frequency range, according to Section 2.3.3, and are shown in Fig. 6. All blends exhibited decreasing permittivity with increasing frequency, with a noticeable relaxation occurring near 10^5 Hz, consistent with dipolar relaxation associated with the glass transition of the amorphous phase [40].

At 1 kHz, ε_r of the neat terpolymer was 28, comparable to values reported for P(VDF-TrFE-CTFE) films prepared from MEK and annealed under similar conditions (110 °C, 2 h) [21,34]. This remains near the lower bound of the 30–60 interval (1 kHz) reported in the material datasheet [41]. With increasing P(VDF-TrFE) content, ε_r decreased to 24 (10 wt%), 21 (20 wt%) and 15 (30 wt%), consistent with previously reported terpolymer blends [24,42]. This behavior can be attributed to the incorporation of a low-ε_r copolymer in a high-ε_r relaxor terpolymer matrix [14]. This effect is likely further enhanced by the high VDF content of the specific P(VDF-TrFE) 70/30 copolymer studied here, as more VDF-rich P(VDF-TrFE) compositions have been associated with stronger ferroelectric character and lower room-temperature permittivity [43].

The loss tangent also decreased with increasing copolymer content across the whole frequency range, with the decrease becoming more pronounced at higher frequencies, where the dielectric response is more sensitive to dipole mobility. For instance, $\tan\delta$ decreased from 0.42 in the neat terpolymer to 0.31 in the 30 wt% blend at 1 MHz, compared with a smaller decrease from 0.065 to 0.053 at 1 kHz.

3.4 Chain conformation

ATR-FTIR measurements were conducted as described in Section 2.3.4, and similar changes with composition were observed for both film thicknesses. The normalized absorbance spectra of the neat terpolymer and its blends with P(VDF-TrFE) are plotted in Fig. 7.

The terpolymer exhibits different chain conformations consisting of *trans* and *gauche* segments, including $T_{m>3}$ conformation at 847 and 1290 cm^{-1}, a $TGTG'$ contribution near 613 cm^{-1}, and a low-wavenumber band near 504 cm^{-1}. While the latter band has previously been assigned to T_3GT_3G', recent studies suggest that it is more accurately described as a disordered 3/1-helical $(TG)_3$ conformation [44–46].

The relation between these low-wavenumber bands and relaxor behavior is treated differently in the literature, with the 504 cm^{-1}

Table 1

Summary of transducer tip displacements (δ), material strains (S), stresses (σ), energy densities (U_S) and actuation efficiency (k_u^2) at 20 V/μm (1 Hz).

Material[a]	δ (mm)	S (%)	σ (kPa)	U_s (kJ/m^3)	k_u^2 ($\times 10^{-4}$)
0 wt%	0.352–1.08	0.045–0.138	54–166	0.012–0.115	0.13–1.26
10 wt%	0.741–2.135	0.083–0.240	115–332	0.048–0.398	0.69–5.76
20 wt%	0.542–0.982	0.047–0.086	87–158	0.020–0.068	0.43–1.43
30 wt%	0.572–0.940	0.041–0.067	96–157	0.020–0.053	0.71–1.92

[a] Mass fraction of P(VDF-TrFE) in the blends.

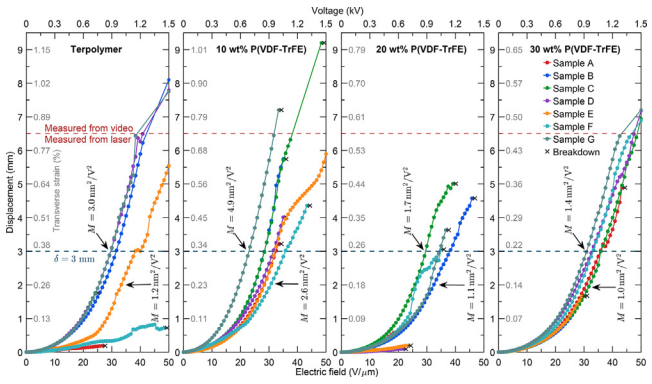

Fig. 8

Actuator maximum tip displacements at incrementally increasing electric field amplitudes (1 Hz sine excitation) for each EAP composition. Up to 3 mm displacements (marked in dashed line) are used for strain analysis and maximum displacements above 6.5 mm were identified from video.

band often linked to intrinsic relaxor ferroelectricity in PVDF-based EAPs [45–47], while studies on terpolymer blends mainly relate the 613 cm^{-1} *TGTG′* band to relaxor behavior [24,25].

Upon blending with P(VDF-TrFE), the integrated absorbance of the 504 and 613 cm^{-1} bands gradually decreased, whereas the bands at 847 and 1290 cm^{-1} increased monotonically with copolymer content. These results indicate that P(VDF-TrFE) addition promotes longer *trans* sequences characteristic of the ferroelectric β phase while suppressing *trans–gauche* chain conformations associated with relaxor properties, in agreement with recent work by Van Duong *et al.* on similar blends [25].

3.5 Transduction

3.5.1 Quasi-static actuation

Actuator tip displacements in the quasi-static experiments (1 Hz sine excitation) are summarized in Fig. 8 and Table 1. Compared to the neat terpolymer, only the 10 wt% P(VDF-TrFE) blend produced improved displacements, while the higher copolymer contents (20 and 30 wt%) led to slight reduction in actuation. At a 20 V/μm field strength, the 1.08 mm displacement in neat terpolymer increased to 2.1 mm in the 10 wt% blend and decreased to 0.982 and 0.940 mm respectively in the 20 and 30 wt% formulations. At higher fields (40–50 V/μm), the highest tip displacements (up to 9.2 mm) were exhibited by the 10 wt% blends (see images in Fig. 9), followed by the neat terpolymer (8.1 mm) and the 30 wt% blends (7.2 mm). In contrast, the 20 wt% actuators produced only up to 5.0 mm deflection, and 6 out of 7

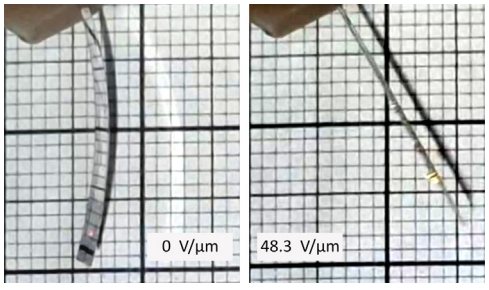

Fig. 9

Actuation response to 48.3 V/μm excitation (1 Hz, 1.45 kV) in 10 wt% copolymer blend samples.

Table 2

Fit parameters for $S = ME^2$ within the $\delta \leq 3$ mm range.

Material[a]	2–20 V/μ m		2–40 V/μ m	
	M[b]	R^2	M[b]	R^2
0 wt%	1.23–2.98	0.983–0.978	1.28–3.22	0.656–0.917
10 wt%	2.59–4.94	0.898–0.957	2.41–5.02	0.987–0.938
20 wt%	1.10–1.71	0.995–0.946	1.19–1.88	0.828–0.825
30 wt%	1.01–1.45	0.991–0.975	1.08–1.57	0.877–0.878

[a] Mass fraction of P(VDF-TrFE) in the blends.
[b] M is given in nm^2/V^2.

samples failed below 40 V/μm, likely due to manufacturing defects (e.g. top-electrode cracks and bubbles, pores, and dust particles in the EAP films).

The apparent electrostrictive coefficients indicated in Fig. 8 were obtained by fitting $S = ME^2$ using S estimated from Eq. (4), and the corresponding R^2 values are summarized in Table 2. M is the highest for the 10 wt% blends ($M =$ 2.6–4.9 nm^2/V^2), followed by the neat terpolymer ($M =$ 1.2–3.0 nm^2/V^2), and decreases for the 20 wt% ($M =$ 1.1–1.7 nm^2/V^2) and 30 wt% ($M =$ 1.0–1.4 nm^2/V^2) formulations. These transduction coefficients (and later the film stresses and transduction efficiencies) were calculated only for $\delta \leq 3$ mm, as they depend on in-plane strains that can be reliably calculated from Eq. (4) only for small deflections (see Section 2.3.5).

The transverse strains for $\delta \leq 3$ mm are plotted against the electric field strength in Fig. 10, where most samples exhibit an approximately quadratic response below 20 V/μm (see Table 2). Deviations from this behavior become pronounced at higher strains due to gradual deviation from a linear deflection-strain relation (Eq. (4)) and at higher field strengths due to the samples

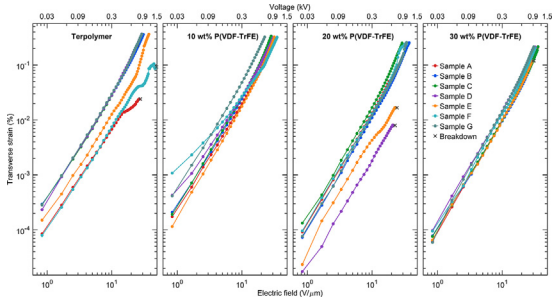

Fig. 10

Transverse strain versus electric field strength. Strains were calculated from the experimentally measured tip deflections (1 Hz, $\delta \leq 3$ mm) using Eq. (4).

nearing their breakdown. The latter is hypothesized to be caused by the localized fabrication defects, where the field strength is much higher than elsewhere in the sample. Near breakdown, these defects start drawing current, reducing actuation via locally or globally lowered field strength across the electrodes. At lower field strengths, these defects have limited effect on actuation, since their surface area forms a negligible fraction of the total actuator area.

Maximum strains in Fig. 10 decrease with copolymer content because the strain-deflection relation (Eq. (4)) is a function of EAP Young's modulus that varies with P(VDF-TrFE) content (Fig. 5). The spread between lower- and upper-bound responses in Figs. 8 and 10 is attributed mainly to sample-to-sample manufacturing variability (stencil-printing is a manual process). The lower bounds are likely affected by fabrication defects and the upper bounds are closer to the intrinsic material response limits. This spread decreases with increasing P(VDF-TrFE) content, especially in the 30 wt% formulation, suggesting improved manufacturing repeatability or reduced defect sensitivity in the stiffer blends.

Low-voltage cyclic actuation is shown in Fig. 11 for the four EAP compositions upon 200 V excitation (6.7 V/μm) at two operating frequencies (0.1 and 1 Hz). At 0.1 Hz, the neat terpolymer actuators showed deflections of up to 108 μm, increasing to 160 μm for the 10 wt% blend and decreasing to 92 and 105 μm for the 20 and 30 wt% blends, respectively. At 1 Hz, a small reduction (5–7%) was observed in the deflection amplitude of all actuators (see Section 3.5.3). While the plots show additional resonant responses due to ground vibrations and displacement bias due to 100 V bias in the 200 V input, copolymer addition did not cause observable broadening in the hysteresis loops.

3.5.2 *Film stress and actuator efficiency*

The EAP film stresses (σ) and energy densities (U_S) are plotted against the field strengths in Fig. 12 and summarized in Table 1. At 20 V/μm the 10 wt% copolymer blend exhibits an increased σ (332 kPa) and U_S (0.398 kJ/m^3) compared to the neat terpolymer (166 kPa and 0.115 kJ/m^3 respectively), while the 20 w% and 30 w% blends show an incremental reduction is both the film stresses (up to 158 kPa and 157 kPa respectively) and energy densities (up to 0.068 kJ/m^3 and 0.053 kJ/m^3 respectively).

Table 3

Summary of actuator dynamics parameters extracted from Fig. 14.

Material[a]	δ_{qs} (mm)	δ_{res} (mm)	f_{res} (Hz)	Q (-)
0 wt%	0.041–0.100	0.562–1.502	20.03–25.22	8.00–13.11
10 wt%	0.040–0.150	0.355–2.309	17.18–25.22	6.10–14.94
20 wt%	0.054–0.080	0.581–1.531	15.91–27.24	7.70–15.78
30 wt%	0.056–0.090	0.635–1.340	18.55–23.36	6.92–15.23

[a] Mass fraction of P(VDF-TrFE) in the blends.

Improved actuation properties upon blending P(VDF-TrFE-CTFE) with low concentration of P(VFD-TrFE) are probably caused by a combination of film stiffness and field-induced strain. A recent work on P(VDF-TrFE)/relaxor-terpolymer unimorph actuators, although based on different terpolymer and copolymer compositions, reported a σ maximum at 10 wt% copolymer content (over 0–20 wt% range) and further related it to changes in film nanostructure [25].

Actuator coupling efficiencies (k_u^2, see Eq. (5)) are plotted in Fig. 13, indicating variation between EAP compositions and individual samples, with a near-quadratic field dependence up to 20 V/μm ($k_u^2 \propto E^2$) that becomes superquadratic at higher fields ($k_u^2 \propto E^n$, $n = 2.2 - 2.8$ from fits). Efficiencies at 20 V/μm are further indicated to evaluate the performance at low field strengths, **as** before break-down specifics complicates comparison. The 10 wt% blends exhibited the highest low-field (0.0576% at 20 V/μm) and peak efficiencies (0.0819% at 22.5 V/μm), followed by the 30 wt% blends (0.0192% at 20 V/μm and 0.0742% at 30 V/μm), 20 wt% blends (0.0143% at 20 V/μm and 0.0569% at 29.2 V/μm), and pure terpolymer (0.0126% at 20 V/μm and 0.0423% at 29.2 V/μm). Therefore, the blends showed up to 357% and 93.6% improvement in low-field and peak efficiencies over P(VDF-TrFE-CTFE). While the maximum in k_u^2 at 10 wt% P(VDF-TrFE) follows from the maximum in film stress (Fig. 12), the higher k_u^2 values of the 20 and 30 wt% blends relative to the neat terpolymer likely reflect improved mechanical coupling with the stainless steel substrate and reduced dielectric energy storage due to their lower permittivity (Fig. 6).

3.5.3 *Dynamics*

The frequency response of each actuator was measured at 200 V (6.7 V/μm) excitation, following methodology in Section 2.3.5. The magnitude plots of each four material compositions are given in Fig. 14, and the key results are summarized in Table 3. Actuation responses are dominated by the second-order dynamics of a cantilever beam that is agitated by the field-dependent stresses in the EAP film layer, i.e. they start with a near-flat low-frequency response (see Section 3.5.1), followed by a strongly increased response near the resonance, and a steep roll-off at higher frequencies.

At low frequencies (1 Hz), the neat terpolymer and the blends showed up to 0.1 mm (neat terpolymer), 0.15 mm (10 wt%), 0.08 mm (20 wt%) and 0.098 mm (30 wt%) deflections peak-to-peak. In resonance, the respective figures increased to 1.502 mm (21 Hz, neat terpolymer), 2.309 mm (17.2 Hz, 10 wt%), 1.531 mm (18.5 Hz, 20 wt%) and 1.340 mm (20 Hz, 30 wt%). Resonance

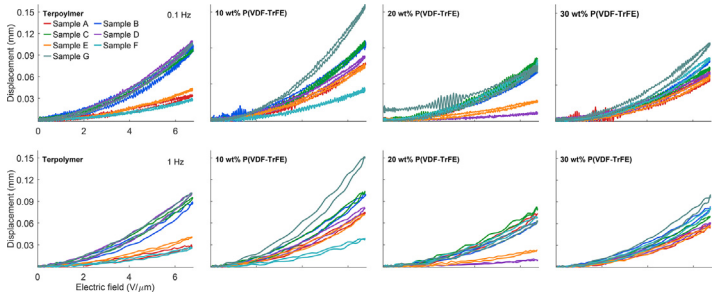

Fig. 11

Actuator tip displacements in response to 200 V (6.7 V/μm) sinusoidal excitation at 0.1 Hz (top row) and 1 Hz (bottom row) frequencies.

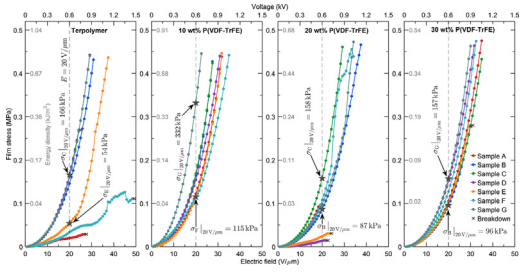

Fig. 12

EAP film stress versus electric field strength (1 Hz, $\delta \leq 3$ mm). Corresponding energy density levels are shown in gray.

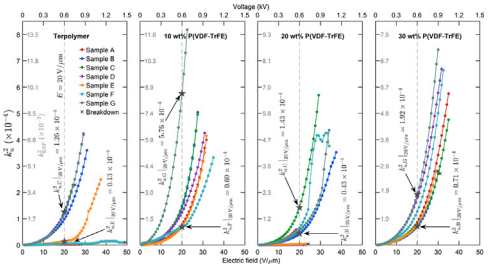

Fig. 13

Transducer efficiency versus electric field strength (1 Hz, $\delta \leq 3$ mm). Corresponding k^2_{EAP} (Eq. (5)) levels are shown in gray.

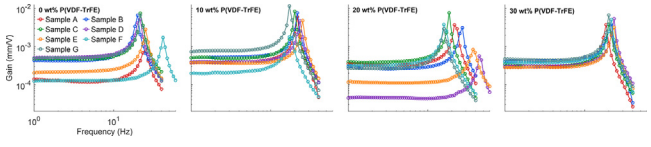

Fig. 14

Frequency response of EAP actuators in the 1–60 Hz range at fixed voltage amplitude (200 V, 6.7 V/μm).

Q-factors (see Table 3) remained in the 6.1 to 15.78 interval. Strongest actuation dynamics were therefore exhibited by the 10 wt% blends, improving the quasi-static and dynamic responses respectively by up to 50% and 53.7% compared to the neat terpolymer.

Resonant frequencies vary significantly between samples (Table 3), and no clear relationship can be observed between the resonant frequency and copolymer concentration (EAP stiffness rises with copolymer content, Fig. 5). This is due to insignificant contribution of the EAP layer to the total sample stiffness (ca $10^3\times$ lower in EAP compared to steel), and more dominant role of the variations in mass distribution due to manufacturing imperfections (non-uniformities at the stencil edges and exact placement of the stencil). Additionally, some samples exhibited significantly higher resonant frequencies, in 40–42 Hz interval, possibly caused by the residual biaxial stresses (EAP shrinkage and steel sheet delivery on rolls) that cause curving in the samples, leading to multi-stable switching near the straight configuration (curving first along the length and then along the width), and increasing the apparent stiffness. Low-field and quasi-static experiments are significantly less sensitive to these effects.

4 Conclusions

This work investigated the actuation properties of EAP blends based on a relaxor-ferroelectric P(VDF-TrFE-CTFE) terpolymer (8.6 mol% CTFE) and a ferroelectric P(VDF-TrFE) copolymer (70 mol% VDF). Blends containing up to 30 wt% copolymer were stencil-printed onto thin steel substrates and thoroughly characterized in dielectric and mechanical properties. Unimorph cantilever actuators were produced for characterizing actuation properties and transduction.

Addition of P(VDF-TrFE) gradually increased the Young's modulus from 120 MPa for the neat terpolymer to 233 MPa for the 30 wt% blends, while dielectric permittivity and dielectric loss tangent decreased with increasing copolymer content in the 100 Hz-1 MHz frequency range. Structurally, P(VDF-TrFE) addition promoted the ferroelectric $T_{m>3}$ conformation while reducing *trans-gauche* contributions related to relaxor properties.

Among the investigated compositions, the 10 wt% blends provided the best overall actuator performance, resulting from the highest film stress (up to 445 kPa, 22.5 V/μm) and strain energy density (up to 0.72 kJ/m^3, 22.5 V/μm). Actuation dynamics of unimorph cantilevers was characterized for up to 60 Hz frequency and 50 V/μm field strength. Unimorph cantilever actuators (20 mm length) showed strongest responses for 10 wt% blends, with up to 9.2 mm displacements (48.3 V/μm, 0.1 Hz) and 0.0819% transducer efficiencies (22.5 V/μm, 0.1 Hz), i.e. a 13.6% and 93.6% improvement over neat terpolymer actuators, respectively. Higher copolymer contents (20 and 30 wt%) showed lower displacements, while increasing in stiffness and actuator efficiency (up to 0.0742% at 30 V/μm in 30 wt% blends). Highest

low-field response (6.7 V/μm) was also seen in 10 wt% copolymer samples, showing a quasi-static response of 0.15 mm (1 Hz) that increases to 2.3 mm at resonance (17.2 Hz), corresponding to a 53.7% improvement over the neat P(VDF-TrFE-CTFE) actuators.

These findings support simple polymer blending as a practical strategy to enhance performance in PVDF-based unimorph actuators. Further improvements are expected through optimization of blend composition and actuator design.

Declaration of competing interest

The authors declare that they have no known competing financial interests or personal relationships that could have appeared to influence the work reported in this paper.

Data availability

Data will be made available on request.

CRediT authorship contribution statement

Giulio Gallucci: Writing – original draft, Visualization, Methodology, Investigation, Formal analysis, Data curation, Conceptualization. **Andres Hunt:** Writing – review & editing, Visualization, Validation, Supervision, Resources, Project administration, Funding acquisition, Conceptualization.

References

[1] Y. Bar-Cohen, Electroactive polymers as artificial muscles: areview, J. Spacecr. Rock. 39 (6) (2002) 822–827, doi:10.2514/2.3902.

[2] D. Narvaez, B. Newell, A review of electroactive polymers in sensing and actuator applications, Actuators 14 (6) (2025), doi:10.3390/act14060258.

[3] T. Levard, P.J. Diglio, S.-G. Lu, C.D. Rahn, Q.M. Zhang, Core-free rolled actuators for braille displays using P (VDF–trFE–CFE), Smart Mater. Struct. 21 (1) (2011) 012001.

[4] W.-E. Ju, Y.-J. Moon, C.-H. Park, S.T. Choi, A flexible tactile-feedback touch screen using transparent ferroelectric polymer film vibrators, Smart Mater. Struct. 23 (7) (2014) 074004, doi:10.1088/0964-1726/23/7/074004.

[5] Q. Van Duong, V.P. Nguyen, F. Domingues Dos Santos, S.T. Choi, Localized fretting-vibrotactile sensations for large-area displays, ACS Appl. Mater. Interface. 11 (36) (2019) 33292–33301, doi:10.1021/acsami.9b09691. PMID: 31411459

[6] S. Ahmed, Z. Ounaies, E.A.F. Arrojado, Electric field-induced bending and folding of polymer sheets, Sens. Actuat. A: Phys. 260 (2017) 68–80.

[7] N. Della Schiava, M.-Q. Le, J. Galineau, F. Domingues Dos Santos, P.-J. Cottinet, J.-F. Capsal, Influence of plasticizers on the electromechanical behavior of a P (VDF-trFE-CTFE) terpolymer: toward a high performance of electrostrictive blends, J. Polym. Sci. B: Polym. Phys. 55 (4) (2017) 355–369.

[8] M.Q. Le, J.-F. Capsal, J. Galineau, F. Ganet, X. Yin, M.D. Yang, J.-F. Chateaux, L. Renaud, C. Malhaire, P.-J. Cottinet, et al., All-organic electrostrictive polymer composites with low driving electrical voltages for micro-fluidic pump applications, Sci. Rep. 5 (1) (2015) 1–13.

[9] K. Koga, H. Ohigashi, Piezoelectricity and related properties of vinylidene fluoride and trifluoroethylene copolymers, J. Appl. Phys. 59 (6) (1986) 2142–2150.

[10] A. Jain, S.J. Kumar, D.R. Mahapatra, V.T. Rathod, Development of P (VDF-trFE) films and its quasi-static and dynamic strain response, Int. J. Eng. Res. Technol. 2 (2013) 2598–2605.

[11] H. Xu, Z.-Y. Cheng, D. Olson, T. Mai, Q.M. Zhang, G. Kavarnos, Ferroelectric and electromechanical properties of poly (vinylidene-fluoride–trifluoroethylene–chlorotrifluoroethylene) terpolymer, Appl. Phys. Lett. 78 (16) (2001) 2360–2362.

[12] F. Xia, Z.-Y. Cheng, H.S. Xu, H.F. Li, Q.M. Zhang, G.J. Kavarnos, R.Y. Ting, G. Abdul-Sadek, K.D. Belfield, High electromechanical responses in a poly (vinylidene fluoride–trifluoroethylene–chlorofluoroethylene) terpolymer, Adv. Mater. 14 (21) (2002) 1574–1577.

[13] J.T. Garrett, C.M. Roland, A. Petchsuk, T.C. Chung, Electrostrictive behavior of poly(vinylidene fluoride-trifluoroethylene-chlorotrifluoroethylene), Appl. Phys. Lett. 83 (6) (2003) 1190–1192, doi:10.1063/1.1600515. https://pubs.aip.org/aip/apl/article-pdf/83/6/1190/18580553/1190_1_online.pdf

[14] G. Gallucci, A. Hunt, Poly(vinylidene fluoride)-based ferroelectric polymers for electromechanical transduction: a systematic review of materials and actuators, Adv. Intell. Syst. 8 (3) (2026) e202500694, doi:10.1002/aisy.202500694.

[15] B. Qiao, X. Wang, S. Tan, W. Zhu, Z. Zhang, Synergistic effects of maxwell stress and electrostriction in electromechanical properties of poly(vinylidene fluoride)-based ferroelectric polymers, Macromolecules 52 (22) (2019) 9000–9011, doi:10.1021/acs.macromol.9b01580.

[16] N.D. Kha Tu, M.-S. Noh, Y. Ko, J.-H. Kim, C.Y. Kang, H. Kim, Enhanced electromechanical performance of P(VDF-trFE-CTFE) thin films hybridized with highly dispersed carbon blacks, Compos. B: Eng. 152 (2018) 133–138, doi:10.1016/j.compositesb.2018.06.036. https://www.sciencedirect.com/science/article/pii/S1359836818313532

[17] A. Javadi, Y. Xiao, W. Xu, S. Gong, Chemically modified graphene/P(VDF-trFE-CFE) electroactive polymer nanocomposites with superior electromechanical performance, J. Mater. Chem. 22 (2012) 830–834, doi:10.1039/C1JM13786G.

[18] J.-F. Capsal, J. Galineau, M. Lallart, P.-J. Cottinet, D. Guyomar, Plasticized relaxor ferroelectric terpolymer: toward giant electrostriction, high mechanical energy and low electric field actuators, Sens. Actuat. A: Phys. 207 (2014) 25–31, doi:10.1016/j.sna.2013.12.008. https://www.sciencedirect.com/science/article/pii/S0924424713005992

[19] G. Gallucci, A. Hunt, Phthalate-free plasticization of electrostrictive P(VDF-trFE-CTFE) for enhanced actuation, ACS Omega 11 (9) (2026) 15254–15268, doi:10.1021/acsomega.5c12507.

[20] N. Della Schiava, F. Pedroli, K. Thetpraphi, A. Flocchini, M.-Q. Le, P. Lermusiaux, J.-F. Capsal, P.-J. Cottinet, Effect of beta-based sterilization on P (VDF-trFE-CFE) terpolymer for medical applications, Sci. Rep. 10 (1) (2020) 8805.

[21] X. Yin, Q. Liu, J. Galineau, P.-J. Cottinet, D. Guyomar, J.-F. Capsal, Enhanced electromechanical performances in plasticizer modified electrostrictive polymers, Eur. Polym. J. 76 (2016) 88–98, doi:10.1016/j.eurpolymj.2016.01.030. https://www.sciencedirect.com/science/article/pii/S0014305716300295

[22] L.J. Gorny, S.-G. Lu, S. Liu, M. Lin, Electromechanical properties of relaxor ferroelectric P(VDF-trFE-CFE)-p(VDF-CTFE) blends, IEEE Trans. Ultrason. Ferroelectr. Freq. Control 60 (3) (2013) 441–445, doi:10.1109/TUFFC.2013.2587.

[23] B. Chu, B. Neese, M. Lin, X. Zhou, Q. Chen, Q.M. Zhang, Improvement of dielectric energy density in PVDF terpolymer nanocomposites and blends, TechConnect Br. Technical Proceedings of the 2008 Clean Technology Conference and Trade Show (2008) 499–502.

[24] Q.V. Duong, C. Park, Y. Lee, S. Lee, T.T. Nguyen, V.P. Nguyen, K. Lee, F.D.D. Santos, C. Park, S.T. Choi, High-temperature electromechanical actuation of relaxor ferroelectric polymers blended with normal ferroelectric polymer, Giant 17 (2024) 100208, doi:10.1016/j.giant.2023.100208. https://www.sciencedirect.com/science/article/pii/S266654252300070X

[25] Q.V. Duong, N. Her, F. Domingues Dos Santos, S.T. Choi, Influence of CTFE content and P(VDF-trFE) copolymer blending on actuation performance of relaxor ferroelectric P(VDF-trFE-CTFE) terpolymers, Mater. Lett. 405 (2026) 139746, doi:10.1016/j.matlet.2025.139746. https://www.sciencedirect.com/science/article/pii/S0167577X25017768

[26] Y.-L. Shen, Nanoindentation for Testing Material Properties, Springer Singapore, Singapore, pp. 1981–2012. 10.1007/978-981-10-6884-3_46

[27] C.M. Roland, J.T. Garrett, R. Casalini, D.F. Roland, P.G. Santangelo, S.B. Qadri, Mechanical and electromechanical properties of vinylidene fluoride terpolymers, Chem. Mater. 16 (5) (2004) 857–861, doi:10.1021/cm034822h.

[28] P. Celli, S. Gonella, V. Tajeddini, A. Muliana, S. Ahmed, Z. Ounaies, Wave control through soft microstructural curling: bandgap shifting, reconfigurable anisotropy and switchable chirality, Smart Mater. Struct. 26 (3) (2017) 035001, doi:10.1088/1361-665X/aa59ea.

[29] B.S. Isik, F. Altay, E. Capanoglu, The uniaxial and coaxial encapsulations of sour cherry (prunus cerasus l.) concentrate by electrospinning and their in vitro bioaccessibility, Food Chem. 265 (2018) 260–273, doi:10.1016/j.foodchem.2018.05.064. https://www.sciencedirect.com/science/article/pii/S0308814618308719

[30] C. Camus, P.-J. Cottinet, C. Richard, Design optimization of piezocomposites using a homogenization model: from analytical model to experimentation, Sensors 24 (6) (2024), doi:10.3390/s24061957.

[31] Q.-M. Wang, L.E. Cross, Performance analysis of piezoelectric cantilever bending actuators, Ferroelectrics 215 (1) (1998) 187–213, doi:10.1080/00150199808229562.

[32] Q.-M. Wang, L.E. Cross, Tip deflection and blocking force of soft PZT-based cantilever RAINBOW actuators, J. Am. Ceram. Soc. 82 (1) (1999) 103–110.

[33] Q.-M. Wang, X.-H. Du, B. Xu, L.E. Cross, Electromechanical coupling and output efficiency of piezoelectric bending actuators, IEEE Trans. Ultrason. Ferroelectr. Freq. Control 46 (3) (1999) 638–646, doi:10.1109/58.764850.

[34] Q. Liu, C. Richard, J.-F. Capsal, Control of crystal morphology and its effect on electromechanical performances of electrostrictive P(VDF-trFE-CTFE) terpolymer, Eur. Polym. J. 91 (2017) 46–60, doi:10.1016/j.eurpolymj.2017.03.046. https://www.sciencedirect.com/science/article/pii/S001430571631672X

[35] A. Ferreira, J. Silva, V. Sencadas, J.L.G. Ribelles, S. Lanceros-Méndez, Poly[(vinylidene fluoride)-co-trifluoroethylene] membranes obtained by isothermal crystallization from solution, Macromol. Mater. Eng. 295 (6) (2010) 523–528, doi:10.1002/mame.201000020.

[36] J.H. Park, Y.-C. Nho, M.G. Kang, Dye-sensitized solar cells containing polymer film with honey-comb like morphology, J. Photochem. Photobiol. A: Chem. 203 (2) (2009) 151–154, doi:10.1016/j.jphotochem.2009.01.010. https://www.sciencedirect.com/science/article/pii/S1010603009000276

[37] J.-Y. Sohn, J.-S. Im, J. Shin, Y.-C. Nho, PVDF-HFP/PMMA-coated PE separator for lithium ion battery, J. Solid State Electrochem. 16 (2012) 551–556.

[38] Y. Tian, H. Ding, Q. Jiao, Y. Shi, Influence of solvents on the formation of honeycomb films by water droplets templating, Macromol. Chem. Phys. 207 (5) (2006) 545–553, doi:10.1002/macp.200500462.

[39] K.J. Yoon, J.H. Chung, N.S. Goo, H.C. Park, Thermal deformation and residual stress analysis of lightweight piezocomposite curved actuator device, in: C.S. Lynch (Ed.), Smart Structures and Materials 2001: Active Materials: Behavior and Mechanics, volume 4333, International Society for Optics and Photonics, SPIE, 2001, pp. 418–425, doi:10.1117/12.432781.

[40] Y. Wang, S.-G. Lu, M. Lanagan, Q. Zhang, Dielectric relaxation of relaxor ferroelectric P(VDF-trFE-CFE) terpolymer over broad frequency range, IEEE Trans. Ultrason. Ferroelectr. Freq. Control 56 (3) (2009) 444–449, doi:10.1109/TUFFC.2009.1063.

[41] Piezotech Arkema CRRA, Piezotech RT-TS technical guide, 2020, (Available at: https://page.arkema.com/rs/253-HSZ-754/images/Technical%20Guide%20Piezotech%20RT-TS.pdf.). Accessed 2 July 2026.

[42] D. Thuau, K. Kallitsis, S. Ha, F. Bargain, T. Soulestin, G. Pecastaings, S. Tencé-Girault, F. Domingues Dos Santos, G. Hadziioannou, High and temperature-independent dielectric constant dielectrics from PVDF-based terpolymer and copolymer blends, Adv. Electron. Mater. 6 (3) (2020) 1901250, doi:10.1002/aelm.201901250.

[43] Y. Liu, H. Aziguli, B. Zhang, W. Xu, W. Lu, J. Bernholc, Q. Wang, Ferroelectric polymers exhibiting behaviour reminiscent of a morphotropic phase boundary, Nature 562 (7725) (2018) 96–100.

[44] X.-Z. Chen, X. Li, X.-S. Qian, S. Wu, S.-G. Lu, H.-M. Gu, M. Lin, Q.-D. Shen, Q.M. Zhang, A polymer blend approach to tailor the ferroelectric responses in P(VDF-trFE) based copolymers, Polymer 54 (9) (2013) 2373–2381, doi:10.1016/j.polymer.2013.02.041. https://www.sciencedirect.com/science/article/pii/S0032386113001754

[45] Z. Han, Y. Liu, X. Chen, W. Xu, Q. Wang, Enhanced piezoelectricity in poly(vinylidene fluoride-co-trifluoroethylene-co-chlorotrifluoroethylene) random terpolymers with mixed ferroelectric phases, Macromolecules 55 (7) (2022) 2703–2713, doi:10.1021/acs.macromol.1c02302.

[46] C. Li, Y. Liu, B. Li, Z. Yuan, T. Yang, Y. Liu, H. Gao, L. Xu, X. Yu, Q. Luo, S. Tang, M. Yao, Y. Gong, Z. Fei, L.-Q. Chen, H. Zhang, H. Zhou, Q. Wang, Enhanced energy storage in high-entropy ferroelectric polymers, Nat. Mater. 24 (7) (2025) 1066–1073, doi:10.1038/s41563-025-02211-z.

[47] Y. Liu, B. Zhang, W. Xu, A. Haibibu, Z. Han, W. Lu, J. Bernholc, Q. Wang, Chirality-induced relaxor properties in ferroelectric polymers, Nat. Mater. 19 (11) (2020) 1169–1174, doi:10.1038/s41563-020-0724-6.